

Designing Squaraines to Control Charge Injection and Recombination Processes in NiO-based Dye-Sensitized Solar Cells

Received 00th January 20xx,
Accepted 00th January 20xx

Oliver Langmar,^a Davide Saccone,^b Anna Amat,^c Simona Fantacci,^c Guido Viscardi,^b Claudia Barolo,^{b,*} Rubén D. Costa^{b,†} and Dirk M. Guldi^{b,†}

DOI: 10.1039/x0xx00000x

www.rsc.org/

Herein, the synthesis of a novel family of squaraines (SQ) and their application in p-type dye-sensitized solar cells (DSSC) is presented. In particular, two sets of SQs were designed featuring either two or four anchoring carboxylic groups combined with either oxygen or dicyanovinyl central groups. The SQs have been characterized by using a joint theoretical, photophysical and electrochemical approach. Importantly, the presence of different central groups forces them into a frozen *cis* (dicyanovinyl group) or a *trans* (oxygen group) conformation. Based on the latter, the current work enables the direct comparison between *cis* and *trans* isomers, as well as the impact of a different number of anchors. Considering their electron accepting and light harvesting character they were tested in NiO-based DSSCs. Photocurrent-voltage, incident photon-to-current conversion efficiency, and electrochemical impedance spectroscopy measurements were performed. By virtue of their different symmetry, stereochemistry, and number of carboxylic groups, altered adsorption behavior onto NiO electrodes, as well as diverse charge injection and charge recombination dynamics were noted under operation conditions. SQs with four linkers in a frozen *cis* isomery show the best balance between charge injection and recombination among the investigated SQs, providing a valuable guideline for the molecular design of future SQs for p-type DSSCs. As a complement, we assembled tandem-DSSCs based on our novel SQ sensitizers as low energy absorbers and N719 as high energy absorbing sensitizer. The resulting devices show a complete coverage of the visible light spectrum in the IPCE, due to the combined absorption of the SQ and N719-based photosensitizer.

Introduction

Owing to the ever-increasing demand for energy, new ways are sought to optimize the power conversion of solar technology. To this end, the dye-sensitized solar cell (DSSC) concept is a leading example.¹ A promising approach to increase the conversion efficiency is the design of tandem DSSCs (t-DSSCs), which combine both n- and p-type DSSCs using, for example, TiO₂-based photoanodes and NiO-based photocathodes, respectively.² In a t-DSSC device configuration, both electrodes are decorated with photosensitizers featuring complementary light harvesting properties, covering a maximum range of the visible region of the solar spectrum.² Up to date, the efficiency of t-DSSCs seems to be limited by the performance of the photocathode. In contrast to n-type DSSCs, research on p-type based DSSCs is still in its infancy with maximum efficiencies of only 0.6% based on the I/I₃⁺ redox couple.³ Current activities in the area of p-type DSSCs focus on developing novel photosensitizers to improve the general device performance, whereby a number of key requirements need to be met: (i) a broad absorption spectrum with a high extinction coefficient should be guaranteed; (ii) the highest-occupied molecular orbital (HOMO) energy of the sensitizer must lie below the valence band (VB) energy of the p-type semiconductor; (iii) the lowest-unoccupied molecular orbital

(LUMO) energy should be placed above the redox potential of the electrolyte to ensure efficient electron injection and regeneration, respectively; (iv) a high photo- and thermal-stability is required.⁴ Considering that one of the most efficient dyes for photoanodes are based on Ruthenium(II) complexes,⁵ which absorb in the high-energy region of the visible spectrum, a matching photosensitizer for photocathode in a t-DSSC should harvest light in the low-energy region. In this context, squaraines (SQ) have been widely investigated as near infrared (NIR) light harvesters. As a matter of fact, SQs have turned into promising sensitizers for n-type DSSCs with remarkable efficiencies.⁶ This is in stark contrast to the lack of examples for SQs applied in NiO-based DSSCs.^{7,8} As a matter of fact, since SQs show high extinction coefficients, excellent photostabilities due to the rigidity of the squaraine core, and easy tunability of their molecular and electronic structures,⁹ they seem to fulfill most of the aforementioned key requirements.

As shown in research on n-type DSSC, the symmetry and number of carboxylic groups of the SQ-photosensitizers exerts a drastic impact on the charge injection and/or recombination processes under operation conditions, resulting in a high impact on the device figures-of-merit. Here, the use of VG1 and VG10 resulted in energy conversion efficiencies of 4.6% and 6.1%, respectively.^{10,11}

In the current work, we provide insights into the design of SQs as integrative components for p-type DSSCs, which is, to the best of our knowledge, absent in the literature. We opted for the synthesis of two novel families of SQs - see **Figure 1** - which differ in their structural conformation due to the nature of the central group - oxygen (**O**) versus dicyanovinyl (**CN**) - and the number of carboxylic anchoring groups - two (**2**) versus four (**4**). On one hand, unsymmetric (**O2** and **CN2**) and symmetric (**O4** and **CN4**) SQs are compared to investigate the impact of the number of anchoring groups. On the other hand, introducing

^a Department of Chemistry and Pharmacy, Friedrich-Alexander-Universität Erlangen-Nürnberg, Egerlandstr. 3, 91058 Erlangen, Germany
Email: ruben.costa@fau.de, dirk.guldi@fau.de

^b Department of Chemistry and NIS Interdepartmental Centre, University of Torino, Via Pietro Giuria 7, 10125 Torino, Italy. Email: claudia.barolo@unito.it

^c Computational Laboratory for Hybrid/Organic Photovoltaics (CLHYO), CNR-ISTM, via Elce di Sotto 8, 06123 Perugia, Italy.

[†] Footnotes relating to the title and/or authors should appear here. Electronic Supplementary Information (ESI) available: [details of any supplementary information available should be included here]. See DOI: 10.1039/x0xx00000x

the CN central moiety allows the control over the molecular stereoisomerism, showing either a *cis/trans* equilibrium (**O2** and **O4**) or a frozen *cis* structure (**CN2** and **CN4**). All SQs were investigated by theoretical, photophysical, and electrochemical characterization, and they were employed as photosensitizers in NiO-based DSSCs. Based on current-voltage (J-V), incident photon-to-current conversion efficiency (IPCE), and electrochemical impedance spectroscopy (EIS) assays, we document that the symmetry and the preferred stereoconformation of the SQs rule the adsorption behavior and, in turn, the charge injection and recombination processes under device operation conditions. Complementing this, we assembled t-DSSCs based on our novel SQ-sensitizers as low energy absorber and N719 as high energy absorber, achieving an absorption coverage of the whole visible light spectrum.

Results and Discussion

Synthesis

The structures of **O2**, **O4**, **CN2**, and **CN4** are based on the combination of an electron accepting squaric core and either one or two electron donating biphenylamines. The incentive for their synthesis is to shed some light onto the number of carboxylic anchoring groups and the structural isomerism on the performance of p-type DSSCs.

To maximize the synthetic yields we have modified the previously published procedure by Chang *et al.* on the synthesis of SQs for NiO-based p-type DSSCs.⁷ In particular, we replaced the Suzuki coupling reaction by a Buchwald-Hartwig coupling reaction to link an indolenine moiety to biphenylamine. This helps to reduce the number of synthetic steps to two and places the squaric core between the biphenylamine and the indolenine moieties. Noteworthy, the synthesis of symmetrical SQs is more efficient in terms of time, use of reagents, and costs than the asymmetrical ones, since the formation of hemisquarate intermediates and their subsequent hydrolysis is circumvented. However, it is still under debate in the design of SQs for n-type DSSCs, if asymmetrical dyes might enhance the device performance compared to the symmetric ones.^{10,11} In this context, the use of a microwave heating in a series of synthesis steps, such as indolenine formation and relative alkylation,¹²

palladium-catalyzed heterocoupling reactions, and squarate substitution has enabled to avoid the hydrolysis step between the hemisquarate intermediate and the squaraine formation in the preparation of asymmetric squarines, reducing the reaction time, and enhancing the overall yield.¹³

To sum up the synthesis protocol, 5-bromoindolenine has been synthesized by a Fisher indole reaction starting from 4-bromophenylhydrazine. In the next step, 5-bromoindolenine has been alkylated on the nitrogen with iodoethane and put in reaction with squaric acid or its ethylester. In the case of **CN2** and **CN4**, ethyl squarate has been modified by a Knoevenagel reaction. The bromo-squaraines have been reacted through a Buchwald-Hartwig reaction to introduce the diphenyl-amino moiety. Carboxylic groups were protected as *tert*-butyl ester and deprotected by trifluoroacetic acid to yield the final products bearing two or four carboxyl-anchoring groups – **Scheme 1**. See the supporting information (SI) for a more detailed description of the synthetic pathway.

Theoretical, photophysical, and electrochemical characterizations

The stereoisomerism is expected to govern the performance of SQ sensitized p-type DSSCs, since it induces peculiar HOMO and LUMO electronic charge distribution and it is responsible of the sensitizer adsorption mode and orientation on the semiconductor. Thus, our first step was to perform density functional theory (DFT) calculations, see SI for computational details, to determine the relative stabilities of the *cis/trans* conformers of **O4** and **CN4**. Calculations showed that *trans-O4* is only 0.65 kcal/mol more stable than *cis-O4*, while the *cis-CN4* is 5.40 kcal/mol more stable than the *trans*-isomer. Based on the computed energy stabilities, we can conclude that the CN-functionalized analogues are reasonably locked in the *cis*-configuration due to steric hindrance, while **O4** is likely to be a mixture of the *trans*- and *cis*-isomers. The optimized molecular structures together with the relative energies of all the possible conformers are shown in **Figure S1**.

In **Figure 2** the HOMOs and LUMOs of the optimized SQs are shown. Interestingly, the HOMO is mainly localized on the squaraine core extending up to the fused phenyl rings and at first glance, all the HOMOs appear quite similar. A closer look reveals, however, that the presence of the CN groups concentrates the electronic distribution on the center of the molecule. The strong electron-withdrawing CN groups in **CN2** and **CN4** enhance the electron accepting character of the squaraine core and, as such, tune the electronic distribution of

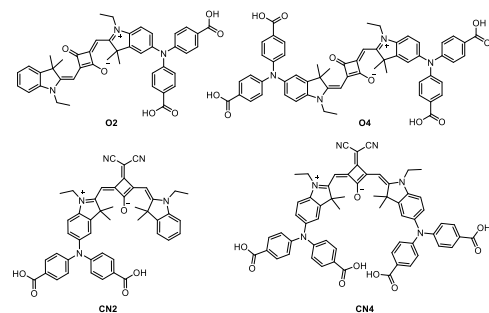
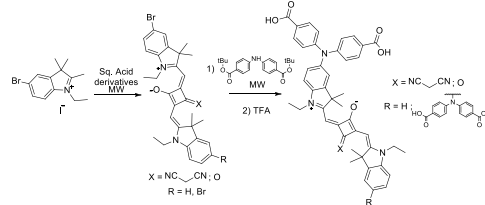


Figure 1: Molecular structures of novel SQ-sensitizers **O2**, **O4**, **CN2**, and **CN4**.



Scheme 1: Synthetic pathway of the novel series of SQs.

the sensitizer.¹⁴ The LUMOs are essentially localized on the squaraine core. Here, the biphenylamines and the dicyanovinyls have, at best, a marginal impact, especially when compared to the trend found for the HOMOs. To go beyond the static representation of electron charge distribution provided by the HOMO-LUMO visualization, we computed the electron density difference in ethanol solution between S_1 state and the ground state of all compounds, see Figure 3. We observe that in conclusion, our results suggest that an efficient electron injection from the NiO electrode into the HOMO orbital of **O2**, **O4**, **CN2**, and **CN4** will set in – a finding that is in excellent agreement with the electrochemical characterization – *vide infra*.

To confirm the electron-accepting character of the novel class of SQs, cyclic voltammetry assays were performed – Figure S2. Two quasi-reversible oxidations centered at around +0.59 and +0.70 V as well as one quasi-reversible reduction in the range from -0.71 to -0.98 V were noted for all SQs (Table 1). Owing to the fact that **O2**, **O4**, **CN2**, and **CN4** give rise to similar reduction features, only minor, if any, differences in the charge injection and electrolyte regeneration driving forces are expected. To solidify this notion, Figure S3 displays an energy diagram gathering the redox features of the SQs along with the Fermi level energy of NiO (+0.5 V)¹⁵ and the redox potential of the I^-/I_3^- redox couple (+0.34 V).¹⁶ Our analyses suggest that both the electron injection from NiO to the excited state of all SQs and the SQ regeneration by the electrolyte are thermodynamically feasible. The only exception is, however, **CN2** which shows a low

driving force of -0.09 V, which is one of the reasons for its low J_{sc} and small IPCE compared to the other sensitizers – *vide infra*. Figure 3 and Table 1 summarize the absorption characteristics of the investigated SQs in solution and on NiO electrodes. **O2** and **O4** show two distinct absorptions at 325 nm ($\epsilon = 8,000 \text{ M}^{-1}\text{cm}^{-1}$) and 650 nm ($\epsilon = 57,100 \text{ M}^{-1}\text{cm}^{-1}$) and at 325 nm ($\epsilon = 22,600 \text{ M}^{-1}\text{cm}^{-1}$) and 674 nm ($\epsilon = 84,600 \text{ M}^{-1}\text{cm}^{-1}$), respectively, ascribable to the S_2 (high-energy region) and the S_1 (low-energy region) transitions.¹⁷ The increased extinction coefficient (ϵ) and the red-shifted absorption spectrum stem from the introduction of a second biphenylamine-moiety and the corresponding change in symmetry, that is, from asymmetric to symmetric. In addition to a general bathochromic shift, a new shoulder emerges at 415 and 400 nm for **CN2** and **CN4**, respectively. Time-dependent DFT calculations (TD-DFT) are consistent with the experimental findings – Table 1. In particular, the low-energy region of the absorption spectra is attributed to a HOMO→LUMO transition. For the **O4**, **CN2**, and **CN4**, the feature in the high-energy region relates to combinations of transitions involving HOMO and HOMO-1 to LUMO, LUMO+2, and LUMO+5 – Table 1, while for **O2** it is due to a single transition with a distinct HOMO-1→LUMO+1 character. For the CN-family, we compute – in line with the experimental observation – an intermediate band at around 400 nm attributed to a single transition from either HOMO-2 or HOMO-3 to LUMO. Finally, since the presence of the CN-moiety forces the SQ bridge into a *cis*-conformation – *vide supra* – a lower ϵ in the case of **CN4** was noted compared to that of **CN2**.

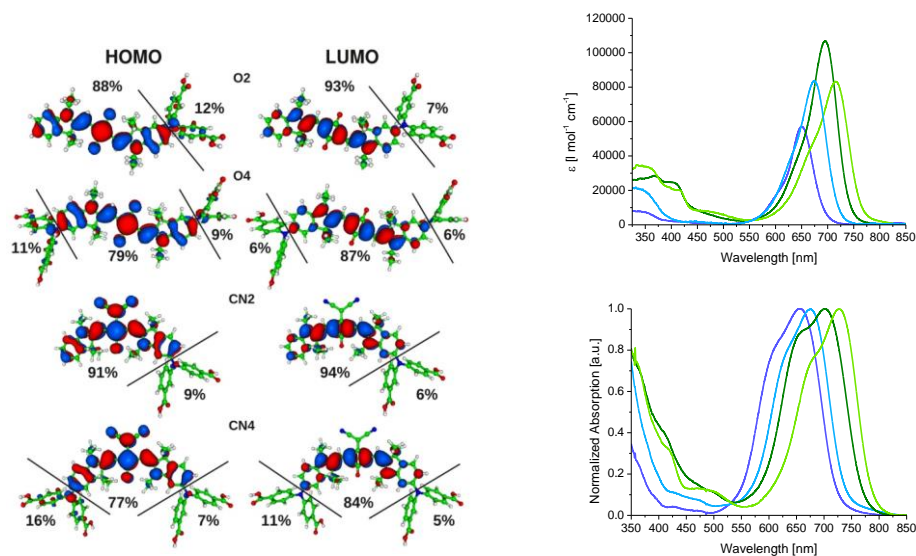


Figure 3: Absorption spectra of O2 (violet), O4 (blue), CN2 (green), and CN4 (light-green) in ethanol (top) and adsorbed onto mesoporous NiO electrodes (bottom).

Table 1: Absorption maxima in solution (λ_{abs}) with their molar extinction coefficient (ϵ), computed absorption maxima (computed λ_{abs}) with their oscillator strengths, nature of the transition, absorption maxima on NiO electrodes (λ_{NiO}), calculated zero-zero transition energy (E_{0-0}), and redox potentials of the investigated.

Dye	λ_{abs} [nm] ($\epsilon \times 10^4 \text{ M}^{-1} \text{ cm}^{-1}$) ^a	Computed λ_{abs} [nm] (osc. str.)	Composition ^b	λ_{NiO} [nm]	E_{0-0} ^c [eV]	Ox_1 ^d [V]	Ox_2 ^d [V]	Red^d [V]
O2	325 (0.80)	338 (0.31)	86% H-1→L+2	655	1.77	+0.69	+0.95	-0.87
	650 (5.71)	586 (1.92)	99% H→L					
O4	325 (2.26)	342 (0.25)	73% H-1→L+3	675	1.71	+0.60	+0.85	-0.98
		366 (0.46)	14% H-2→L+3 64% H-1→L+1 30% H-2→L+1					
			99% H→L					
CN2	674 (8.46)	611 (2.15)	99% H→L	701	1.67	+0.59	+0.80	-0.85
	337 (2.40)	315 (0.21)	67% H→L+5					
	415 (1.46)	346 (0.37)	88% H-1→L+2					
		421 (0.55)	82% H→L+3 92% H-2→L					
CN4	695 (10.72)	613 (1.25)	99% H→L	727	1.61	+0.70	+0.89	-0.71
	366 (2.86)	360 (0.28)	43% H-2→L+1 28% H→L+5 21% H-1→L+1					
		375 (0.36)	87% H→L+4					
	400 (2.48)	402 (0.61)	93% H-3→L					
	714 (4.87)	639 (1.42)	99% H→L					

^a EtOH solutions. ^b This is provided in terms of molecular orbitals with contribution above the 10%. ^c Calculated from the abscissa of the absorption edge with $E_{0-0} = 1238.9/\lambda$. ^d Referenced vs. NHE with $E(\text{Fc}^+/\text{Fc})$ as 0.64V vs. NHE.¹⁸

Corroborating this finding, the extinction coefficient of **O4** increases compared to **O2** as theoretically both the *cis*- and *trans*-conformers are present in solution.

Moreover, the absorption on NiO electrodes was studied – **Figure 3**. Overall, a broadening of the absorption for all SQs and a further red-shift of the maxima due to their binding to NiO electrode surfaces were noted.¹⁹The high-energy shoulder enhanced upon dye adsorption is probably due to thermal and solvent fluctuations as observed in a theoretical study on a squaraine sensitized TiO₂ system. (De Angelis, F.; Fantacci, S.; Gebauer, R. J. Phys. Chem. Lett. 2011, 2, 813–817) More interestingly, the red-shift increases in the order **O4** (1 nm) < **O2** (5 nm) < **CN2** (6 nm) < **CN4** (13 nm). In previous studies, it was documented that the extend of red-shift scales with the strength of interactions with the electrode.^{19,20} Thus, this finding points to a possibly better injection efficiency of **O2** compared to **O4**, as well as for **CN4** compared to **CN2**

p-type DSSC characterization

Next, we assembled p-type DSSCs with NiO-based photocathodes sensitized with the four different SQs. NiO electrodes have been prepared according to literature procedures.²¹ After sintering, the electrodes were immersed for 16 h into 0.1 mM ethanolic solutions of the SQs. Devices were completed with a platinum counter electrode and filled with an electrolyte based on 1 M LiI and 0.2 M I₂ in acetonitrile. The J-V curves and IPCE spectra are shown in **Figure 4**, while the device figures-of-merit are gathered in **Table 2**. Devices have been measured under dark and 1 sun AM 1.5 conditions. As shown in **Figure 4**, the open-circuit voltages (V_{oc} s) and short-circuit current densities (J_{sc} s) decrease from 100.0 to 97.5, to 87.7, and to 85.3 mV and from 1.54 to 1.21, to 1.15, and to 0.94 mA/cm² for devices featuring **O2**, **O4**, **CN4**, and **CN2**, respectively. With almost equal fill factors (FFs) of around 0.35–0.37, the efficiencies differed greatly, namely 0.054% (**O2**), 0.043% (**O4**), 0.029% (**CN2**), and 0.037% (**CN4**). In terms of IPCE, a perfect agreement with the absorption features as shown in **Figure 3** was noted. In the high-energy region, the maximum is mostly dominated by the absorption of the iodine/iodide redox couple, while in the low-energy region, the feature matches with the S₁ transition of the corresponding SQs with values of 8.6%, 3.7%, 3.2%, and 3.0% for **O2**, **CN4**, **CN2**, and **O4**, respectively. To verify the comparability of our results, we looked into the dye loading of all devices. As a matter of fact, the concentrations decrease in the order from 2.02 × 10⁻⁸ (**O4**), to 1.43 × 10⁻⁸ (**O2**), to 0.66 × 10⁻⁸ (**CN4**), and to 0.47 × 10⁻⁸ M (**CN2**). In this context, it seems more decisive to compare SQs with and without the CN moiety rather than the number of anchoring groups.

From the aforementioned figures-of-merit, it is clear that devices sensitized with **O2** outperform any other device, while the increase of anchoring groups (**O4**) correlates with a decrease of the device parameters. In stark contrast, the opposite has been observed for the **CN** family. Here, **CN4** exhibits a better efficiency, as well as higher V_{oc} s and J_{sc} s compared to **CN2** based devices. Helpful is in this regard the

structural conformation and the different dye loading of the SQs on the NiO electrodes. According to the theoretical calculations, **O4** is slightly more stable in its *trans*-conformation. With a seemingly equal dye loading – **Table 2** – it is reasonable to assume that both **O2** and **O4** similarly attach with two linkers upright in a tight manner onto the electrode surface. In stark contrast, **CN4** is most stable in its *cis*-conformation – **Figure 2** – and, thus, both dyes absorb onto NiO in a more bulky manner with either two in the case of **CN2** or with four linkers in the case of **CN4**. These considerations assist in rationalizing a three times lower dye loading relative to **O2** and **O4**. However, both the trend in J_{sc} and η noted in the O-family and the differences in the η between O- and CN-devices cannot be fully explained by the dye loading.

For instance, devices with **O2** and **CN2** dyes showed that the former gives rise to a superior performance in terms of V_{oc} , J_{sc} , and efficiency. This is likely to relate to a higher amount of dye uptake, but an alternative rationale for the lower efficiency of **CN2** devices might include the unfavorable charge shift from the CN-moiety to the SQ core and, in turn, closer to the anchoring group.

Table 2: Figures-of-merit for **O2**, **O4**, **CN2**, and **CN4** p-DSSCs

Dye	V_{oc} [mV]	J_{sc} [mA/cm ²]	FF	η [%]	IPCE [%] ^a	Dye loading [mol/cm ²] ^b
O2	100.0	1.54	0.35	0.054	8.6	1.43 ± 0.19 × 10 ⁻⁸
O4	97.5	1.21	0.36	0.043	3.0	2.02 ± 0.19 × 10 ⁻⁸
CN2	85.3	0.94	0.36	0.029	3.2	0.47 ± 0.04 × 10 ⁻⁸
CN4	87.7	1.15	0.37	0.037	3.7	0.66 ± 0.12 × 10 ⁻⁸

^a Values taken at the corresponding IPCE maxima in the low-energy region of the spectra. ^b Determined from an average of 5 sensitized electrodes.

Commentato [S2]: Based on the optimized molecular geometry of CN4, its adsorption configuration could involve at maximum two linkers, both from the same substituent or from different substituents.

Commentato [S1]: Shifts have to be defined in energy values, since nm is a non-linear unit.

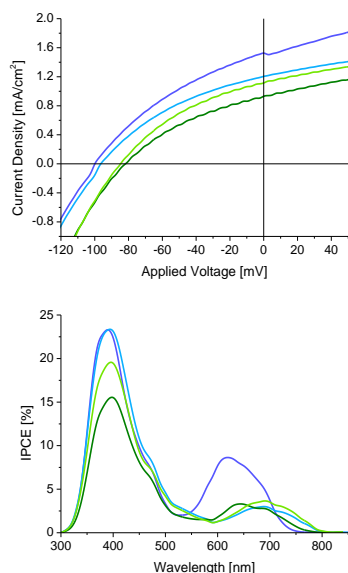


Figure 4: Current density versus applied voltage (top) and incident photon-to-current conversion efficiency (bottom) of devices with **O2** (violet), **O4** (blue), **CN2** (green), and **CN4** (light-green).

As such, charge recombination between the reduced form of **CN2** and the semiconductor surface is facilitated – **Figure 2**. The **O2** versus **CN2** trend is in sharp contrast to the **O4** versus **CN4** trend. Despite a superior dye uptake in the case of **O4**, both devices show nearly the same J_{sc} . Here, we hypothesize that a more balanced charge injection and recombination by virtue of a binding motif that consists of four anchoring groups rather than two is the cause for the reversed trend. Finally, the **CN2** versus **CN4** comparison leads to the same trend. Again, despite comparable dye uptake, four anchoring groups, which are locked into a *cis*-conformation, result in a better balance between charge injection and recombination processes. To corroborate our hypotheses, we turned to electrochemical impedance spectroscopy (EIS) assays. These enabled probing the charge injection and recombination processes under device operation conditions – **Figure 5**.^{22–24} In a Nyquist plot for the p-type DSSC, two semicircles correlate with the resistance across the dye/electrode/electrolyte interface in the low-frequency region and with the platinum/electrolyte interface in the high-frequency region.^{24,25} The electrical circuit model that has been used for the fitting of the obtained Nyquist plots and the calculation of the resistances is shown in **Figure S4**. Under 1 sun AM 1.5 and J_{sc} conditions, the charge-transfer resistance (R_{CT}) clearly relates to the charge injection, since the device runs under maximum photocurrent generation and, thus, recombination is at its minimum.^{23,24} The R_{CT} s under J_{sc}

conditions are 669.2, 648.4, 879.9, and 662.7 Ω for **O2**, **O4**, **CN2**, and **CN4** based-DSSCs, respectively.

Taking the aforementioned into concert, three major conclusions are derived. Firstly, **O2** and **O4** show comparable R_{CT} s, pointing to a similar charge injection. This is only feasible if an analogous attachment onto NiO surfaces is realized – *vide infra*. Therefore, **O4** quite likely attaches *via* only two linkers onto NiO as the **O2** dye. This is feasible since both *cis*- and *trans*-conformations are energetically similar. Secondly, the presence of a CN-moiety fails to improve the charge injection as R_{CT} is higher for **CN2** than for **O2**. On one hand, the dye uptake is inferior and, in therefore, more charges have been injected for **O2**. On the other hand, a charge shift in **CN2** might bring the electron closer to the anchoring group. Thirdly, a nearly 25% higher R_{CT} for **CN2** than for **CN4** points to the superior charge injection process for the latter due to the presence of four anchoring groups, which engage in the adsorption owing to the fact the *cis*-conformation is locked.

Next, EIS assays were performed under dark conditions to gain insights into the recombination resistance (R_{rec}), which mainly correlates with the recombination process between the NiO electrode and the electrolyte. The highest R_{rec} under J_{sc} conditions, namely the least recombination, is found for devices with **CN4** (11,336 Ω) followed by **O2** (10,617 Ω), **CN2** (9,959.8 Ω), and **O4** (7,095.7 Ω). Since **CN4** might attach with four anchoring groups, the best surface coverage of the NiO electrodes leads to the fewest recombination sites for the electrolyte. SQs with only two carboxylic anchors, that is, **O2** and **CN2**, show a comparable rate of recombination with the electrolyte despite differences in the dye uptake. The bulkiness of **CN2** as a means to shield the NiO surface equally good as the more tightly packed **O2**, due to a higher dye loading, seems reasonable. In stark contrast, **O4** shows the highest recombination rate as reflected by a R_{rec} 40% lower compared to **CN4**. Here, an incomplete attachment involving only two rather than four anchoring groups might dominate. This would involve one biphenylamine-moiety, which, for example, points toward the bulk of the electrolyte.

From the EIS measurements under dark and 1 sun AM 1.5 conditions, the effective diffusion length (L_{eff}) and the charge collection efficiency (η_{cc}) have been derived – **Figure S5**.^{22,24,26} L_{eff} and η_{cc} give insights into the ratio of charge injection and recombination of the investigated devices. The earlier is a measure of how far the injected holes travel inside the mesoporous NiO electrode prior to the recombination process, while the latter relates to the amount of injected holes that are collected at the back contact of the device. All devices show increasing L_{eff} s and η_{cc} s upon decreasing the applied voltage. As a matter of fact, this is characteristic for p-type DSSCs.^{22,24} Under V_{oc} conditions, **CN4** shows the longest L_{eff} with 1.21 μm , which decreases to 0.99, to 0.93, and to 0.86 μm for **O2**, **O4**, and **CN2**, respectively. Under the same conditions, η_{cc} increases in the order of 29.3 (**O4**), 42.6 (**O2**), 44.4 (**CN2**), and 44.9% (**CN4**). Considering these parameters, the use of four anchoring groups seems to be only beneficial if the system is locked into a *cis*-conformation (**CN4** versus **O4**).

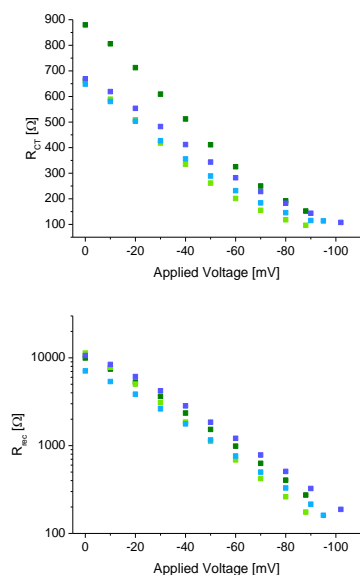


Figure 5: Charge transfer resistance R_{CT} (top) and recombination resistance R_{rec} (bottom) as a function of the applied voltage for **O2** (violet), **O4** (blue), **CN2** (green), and **CN4** (light-green).

After establishing a clear understanding of the impact of the symmetry and number of anchoring group on the device-figures-of-merit, we turned to probe the suitability of our novel SQ-sensitizers in a t-DSSC configuration. We assembled t-DSSCs consisting of TiO_2 as the photoanode, sensitized with N719 as the standard high-energy absorbing sensitizer, and NiO as the photocathode, sensitized with **O2** as the low-energy absorbing sensitizer. The same electrolyte as in the p-DSSC measurements was used (1 M LiI and 0.2 M I_2 in acetonitrile), with the addition of 0.5M 4-*tert*-butylpyridine as a known additive to suppress recombination on the TiO_2 electrode and thus increase the V_{oc} .¹⁶ Furthermore, care has been taken to carefully match the photocurrents of both photoactive electrodes, by reducing the electrode thickness of the TiO_2 -based photoanode – please see the SI for a more detailed description of the device preparation. The J-V curves and IPCE spectra of the single TiO_2 and NiO-based reference devices and of the respective t-DSSC are depicted in **Figure 6** and the device-figures-of-merit in **Table 3**.

As shown in **Figure 6** the TiO_2 and NiO-based reference devices show V_{oc} s of 720.1 and 100.0 mV, J_{sc} s of 1.74 and 1.99 mA/cm^2 FFs of 0.74 and 0.33, and efficiencies of 0.93 and 0.066 %, respectively. In contrast, the respective t-DSSCs show V_{oc} s of 746.2 and 658.3 mV, J_{sc} s of 1.27 and 0.23 mA/cm^2 , FFs of 0.50 and 0.60, and efficiencies of 0.47 and 0.092 % for the illumination by the TiO_2 and NiO-side, respectively. The IPCEs of the reference devices show the typical N719 and **O2** features for the TiO_2 and NiO sensitized-electrodes. Illuminating the t-

DSSC from the TiO_2 side yields an IPCE spectra which is a perfect overlap of the N719 and **O2** features, covering the whole visible spectra from 300 to almost 750 nm. In stark contrast, by illumination from the NiO-side, only weak features of N719 and **O2** are discernible.

From the t-DSSC figures-of-merit, several conclusions can be drawn. Firstly, illuminating the t-DSSC from the TiO_2 -side showed the most promising results with a V_{oc} that is higher than the V_{oc} of the single electrode references and an IPCE spectra which shows the combined features of the sensitized photoanode and photocathode. Both points prove, that our assembled devices work as intended in the t-DSSC configuration being the first t-DSSCs utilizing SQ-based sensitizers for the p-type based photocathode. Secondly, the obtained efficiency and J_{sc} from the TiO_2 -side illumination is

Table 3: Figures-of-merit for the N719/ TiO_2 and O2/NiO reference devices and the respective t-DSSC illuminated from the TiO_2 and NiO side.

Device	V_{oc} [mV]	J_{sc} [mA/cm^2]	FF	η [%]
N719/ TiO_2	720.1	1.74	0.74	0.93
O2/NiO	100.0	1.99	0.33	0.066
t-DSSC TiO_2 side	746.2	1.27	0.50	0.47
t-DSSC NiO side	658.3	0.23	0.60	0.092

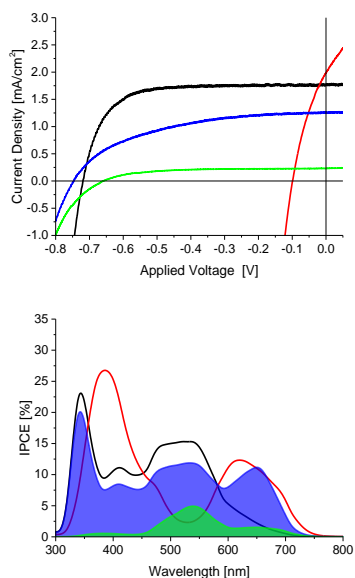


Figure 6: Current density versus applied voltage (top) and incident photon-to-current conversion efficiency (bottom) of the TiO₂ (black) and NiO (red) reference devices and the respective t-DSSC illuminated from the TiO₂ (blue) and NiO (green) side.

lower than that of the TiO₂ reference device. We attribute this, together with the low increase in V_{oc} of the t-DSSC (roughly 25 mV), to the fact, that the electrolyte in our experiment was optimised for the NiO-based photocathode. In general, the here used electrolyte features multiple times higher iodine and iodide concentrations than typical electrolytes for n-type DSSC applications.²⁷ Thus we postulate, that this leads to an increased amount of recombination for the TiO₂-based photoanode in the t-DSSC configuration limiting the obtained V_{oc} and J_{sc} and thus the final device efficiency. Thirdly, illumination from the NiO-side yields generally low device-figures-of-merit. Taking a closer look at the respective IPCE, it is evident that the part around 300 to 450 nm is greatly decreased compared to the t-DSSC illuminated from the TiO₂-side and its n-type reference device. We attribute this to the high absorption of the iodine-based electrolyte in this region, which absorbs most the light that passes through it on its way to the side of the photoanode.^{28,29} Nevertheless, again the features of both the sensitized photoanode and the photocathode can be distinguished by illuminating from the NiO-side, which leads to the conclusion that the t-DSSC is working. Corroborating all this, we show for the first time a t-DSSC which utilizes SQ-sensitizers for the NiO-based photocathode as effective low energy absorbers.

Conclusions

A novel family of SQs for p-type DSSCs, which differ in the number of carboxylic anchoring groups and their conformation due to the introduction of a CN central group, has been synthesized and characterized by means of steady-state photophysical, electrochemical, and computational techniques. DSSCs based on NiO photocathodes and SQs have been assembled and tested. The different conformations of the SQs governed the adsorption onto the electrode surface, which was directly reflected in the dye loading and device efficiency. As a complement, EIS assays were performed to probe the impact of the molecular structures on the electron injection and recombination processes in the device. Here, our findings revealed a better balance between charge injection and recombination for SQs featuring four anchoring groups (CN4) only when a frozen *cis*-conformation is guaranteed. As a complement, we assembled for the first time t-DSSC based on our novel SQs which a complete coverage of the visible light spectrum in the IPCE. Future investigations will involve the synthesis and characterization of symmetric SQ sensitizers to further enhance the charge injection properties under device operation conditions, as well as, the further optimization of SQ-based t-DSSCs

Acknowledgements

R.D.C., O.L., and D.M.G. acknowledge funding from DFG Cluster of Excellence 'Engineering of Advanced Materials' (EAM). Authors thank MIUR-PRIN-2010 20104XET32 "DSSCX" for financial support.

Notes and references

- 1 B. O'Regan and M. Grätzel, *Nature*, 1991, **353**, 737–740.
- 2 A. Nattestad, A. J. Mozer, M. K. R. Fischer, Y. Cheng, A. Mishra, P. Bäuerle and U. Bach, *Nat. Mater.*, 2010, **9**, 31–35.
- 3 X. L. Zhang, Z. Zhang, D. Chen, P. Bäuerle, U. Bach and Y.-B. Cheng, *Chem. Commun.*, 2012, **48**, 9885–9887.
- 4 F. Odobel, L. Le Pleux, Y. Pellegrin and E. Blart, *Acc. Chem. Res.*, 2010, **43**, 1063–1071.
- 5 J. F. Yin, M. Velayudham, D. Bhattacharya, H. C. Lin and K. L. Lu, *Coord. Chem. Rev.*, 2012, **256**, 3008–3035.
- 6 C. Qin, W.-Y. Wong and L. Han, *Chem. Asian J.*, 2013, **8**, 1706–1719.
- 7 C. Chang, Y. Chen, C. Hsu, H. Chou and J. T. Lin,

- Org. Lett.*, 2012, **14**, 4726–4729.
- 8 J. Warnan, J. Gardner, L. Le Pleux, J. Petersson, Y. Pellegrin, E. Blart, L. Hammarström and F. Odobel, *J. Phys. Chem. C*, 2014, **118**, 103–113.
- 9 A. Burke, L. Schmidt-Mende, S. Ito and M. Grätzel, *Chem. Commun.*, 2007, 234–236.
- 10 J. Park, C. Barolo, F. Sauvage, N. Barbero, C. Benzi, P. Quagliotto, S. Coluccia, D. Di Censo, M. Grätzel, M. K. Nazeeruddin and G. Viscardi, *Chem. Commun.*, 2012, **48**, 2782–2784.
- 11 J. Park, N. Barbero, J. Yoon, E. D. Orto, S. Galliano, R. Borrelli, J. Yum, D. Di Censo, M. Gr. K. Nazeeruddin, C. Barolo and G. Viscardi, *Phys. Chem. Chem. Phys.*, 2014, **16**, 24173–24177.
- 12 A. J. Winstead, N. Fleming, K. Hart and D. Toney, *Molecules*, 2008, **13**, 2107–2113.
- 13 N. Barbero, C. Magistris, J. Park, D. Saccone, P. Quagliotto, R. Buscaino, C. Medana, C. Barolo and G. Viscardi, *Org. Lett.*, 2015, **17**, 3306–3309.
- 14 F. Odobel and Y. Pellegrin, *J. Phys. Chem. Lett.*, 2013, **4**, 2551–2564.
- 15 J. He, H. Lindström, A. Hagfeldt and L. Sten-Eric, *J. Phys. Chem. B*, 1999, **103**, 8940–8943.
- 16 G. Boschloo and A. Hagfeldt, *Acc. Chem. Res.*, 2009, **42**, 1819–1826.
- 17 U. Mayerhöffer, B. Fimmel and F. Würthner, *Angew. Chemie, Int. Ed.*, 2012, **51**, 164–167.
- 18 C. M. Cardona, W. Li, A. E. Kaifer, D. Stockdale and G. C. Bazan, *Adv. Mater.*, 2011, **23**, 2367–2371.
- 19 P. Qin, M. Linder, T. Brinck, G. Boschloo, A. Hagfeldt and L. Sun, *Adv. Mater.*, 2009, **21**, 2993–2996.
- 20 P. Qin, H. Zhu, T. Edvinsson, G. Boschloo, A. Hagfeldt and L. Sun, *J. Am. Chem. Soc.*, 2008, **130**, 8570–8571.
- 21 S. Sumikura, S. Mori, S. Shimizu, H. Usami and E. Suzuki, *J. Photochem. Photobiol. A Chem.*, 2008, **199**, 1–7.
- 22 Z. Huang, G. Natu, Z. Ji, M. He, M. Yu and Y. Wu, *J. Phys. Chem. C*, 2012, **116**, 26239–26246.
- 23 H. Choi, S. O. Kang, J. Ko, G. Gao, H. S. Kang, M.-S. Kang, M. K. Nazeeruddin and M. Grätzel, *Angew. Chemie, Int. Ed.*, 2009, **48**, 5938–5941.
- 24 O. Langmar, C. R. Ganivet, A. Lennert, R. D. Costa, G. de la Torre, T. Torres and D. M. Guldi, *Angew. Chemie, Int. Ed.*, 2015, **54**, 7688–7692.
- 25 Z. Huang, G. Natu, Z. Ji, P. Hasin and Y. Wu, *J. Phys. Chem. C*, 2011, **115**, 25109–25114.
- 26 M. Adachi, M. Sakamoto and J. Jiu, *J. Phys. Chem. B*, 2006, **110**, 13872–13880.
- 27 J. Wu, Z. Lan, J. Lin, M. Huang, Y. Huang, L. Fan and G. Luo, 2014.
- 28 J. Cong, X. Yang, L. Kloo and L. Sun, *Energy Environ. Sci.*, 2012, **5**, 9180–9194.
- 29 Z. Hongjun, A. Hagfeldt and G. Boschloo, *J. Phys. Chem. C*, 2007, **111**, 17455–17458.

TOC:

Two novel series of squaraines with differences in their stereochemistry and number of anchoring groups have been synthesized and probed as sensitizers in NiO-based dye-sensitized solar cells. These dyes show a different absorption behavior in the NiO electrode surface, which heavily influences the charge injection and recombination properties of the assembled devices, as proved by electrochemical impedance spectroscopy. Additionally, tandem-DSSCs which show the combined IPCE of our novel squaraine sensitizer and the N719 based TiO₂ photoanode, have been assembled and tested.

Oliver Langmar¹, Davide Saccone², Anna Amat³, Simona Fantacci³, Guido Viscardi², Claudia Barolo^{2*}, Rubén D. Costa,^{1*} and Dirk M. Guldi^{1*}

Designing Squaraines to Control Charge Injection and Recombination Processes in NiO-based Dye-Sensitized Solar Cells